CrystEngComm

PAPER

View Article Online
View Journal | View Issue

Cite this: *CrystEngComm*, 2017, **19**, 47

Occurrence of 3D isostructurality in fluorinated phenyl benzamidines†

Dhananjay Dey and Deepak Chopra*

Received 2nd September 2016,
Accepted 15th November 2016

DOI: 10.1039/c6ce01924b

www.rsc.org/crystengcomm

In the current study, we report the existence of 3D isostructurality behaviour in pairs of isomeric molecules existing as *E*–*Z* isomers. The polymorphic forms **E1** and **E2** of (*E*)-2-fluoro-*N*′-(3-phenyl) benzimidamide are individually isostructural with (*E*)-2-fluoro-*N*′-phenylbenzimidamide and (*E*)-2-fluoro-*N*′-(2-fluorophenyl) benzimidamide, respectively. Furthermore, a similar compound, (*Z*)-3-fluoro-*N*′-(4-fluorophenyl) benzimidamide, is isostructural with (*Z*)-4-fluoro-*N*′-(4-fluorophenyl) benzimidamide. The structural feature has been analyzed in terms of the nature and energetics of the equivalent supramolecular building blocks associated with the presence of various intermolecular interactions in the crystal packing. The crystal packing similarities have been investigated quantitatively *via* XPac analysis and the energy vector model. It is noteworthy to observe the presence of a rarely observed N–H···F interaction which plays an important role in the crystal packing of [(*Z*)-3-fluoro-*N*′-(4-fluorophenyl) benzimidamide]/[(*Z*)-4-fluoro-*N*′-(4-fluorophenyl) benzimidamide]. The NCI isosurface signifies the "attractive" nature of the N–H···F and N–H···π interactions and the different types of C–H···F dimeric motifs. An analysis of the two-dimensional fingerprint plots also provides a quantitative understanding of the occurrence of isostructurality in these compounds.

Introduction

The design of novel supramolecular architectures utilizing non-covalent interactions in the development of novel pharmaceutical compounds is the current interest in crystal engineering.[1] It is important to understand the role of intermolecular interactions in the design of similar molecular arrangements having equivalent structural motifs in molecular crystals.[2] The control of the mutual arrangement of the molecules in the solid state to obtain the desired characteristics utilizing the intermolecular interactions is the art of crystal engineering.[3,4] According to the IUCr definition of isostructurality, "Two crystals are said to be isostructural if they have the same structure, but not necessarily the same unit-cell dimensions nor the same chemical composition, with a comparable variability in the atomic coordinates to that of the cell dimensions and chemical composition".[5] It is of interest to study the phenomenon of isostructurality in isostructural polymorphs,[6–11] isostructural co-crystals[1,12,13] and isostructural solvates[14] on account of their applications in the pharmaceutical industry.[15–20] This behaviour is very common in similar related compounds having different types of structural equivalent functionalities like –H, $–CH_3$, –F, –Cl, –Br and I.[21–23] Gelbrich and co-workers have studied fourteen crystal structures of 4,5′-substituted benzenesulfonamido-2-pyridines with interchange of the substituent having those functionalities and observed the robustness of the supramolecular architectures having N–H···N bonded centrosymmetric dimers in three-dimensional (3D) isostructural molecular arrangement.[23] Similarly related compounds can also exhibit 1D (one-dimensional) and 2D (two-dimensional) isostructural similarity instead of 3D (three-dimensional) isostructurality.[24,25]

N-Aryl benzamidines are an important class of compounds having interesting biological properties, including inhibitor activity towards tyrosine kinases[26] and nitric oxide synthases,[27] and can act as selective D_1 dopamine receptor antagonists.[28] In addition, antimicrobial[29] and antiparasitic[30–32] activities have also been reported.[33] The presence of the fluorine atom in the molecule is responsible for the better physicochemical properties, chemical reactivity, and biological activity compared to the non-fluorinated analogues.[34–37] Organic fluorine has been observed to behave differently in an organic environment, and its contribution in the context of crystal engineering is now widely established.[38]

Crystallography and Crystal Chemistry Laboratory, Department of Chemistry, Indian Institute of Science Education and Research Bhopal, Bhopal By-Pass Road, Bhauri, Bhopal-462066, Madhya Pradesh, India. E-mail: dchopra@iiserb.ac.in; Fax: +91 755 6692392

† Electronic supplementary information (ESI) available. CCDC 982077, 982078, 982081 and 982085. For ESI and crystallographic data in CIF or other electronic format see DOI: 10.1039/c6ce01924b

Experimental

Synthesis

In this study, we have synthesized the four fluorinated benzamidine compounds (Schemes 1 and 2) **DB10** [(*E*)-2-fluoro-*N*′-phenylbenzimidamide], **DB11** [(*E*)-2-fluoro-*N*′-(2-fluorophenyl) benzimidamide], **DB23** [(*Z*)-3-fluoro-*N*′-(4-fluorophenyl) benzimidamide] and **DB33** [(*Z*)-4-fluoro-*N*′-(4-fluorophenyl) benzimidamide]. For this, a round bottom flask (10 mL) containing a stirrer bar and 0.70 g of powdered anhydrous aluminium chloride (~1.2 eq.) was charged with 1 eq. of fluorinated benzonitrile at room temperature (25 °C) in a silicon oil bath placed on a magnetic stirrer. A guard tube (filled with anhydrous calcium carbonate) was attached on top of the round bottom flask. Then the mixture was heated up to 100 °C until a homogeneous melt (aluminium chloride–fluorobenzonitrile complex) was formed. After 30 minutes, 1 eq. of fluorinated aniline was added at a time into the melted mixture by using a syringe. The temperature was increased up to 120 °C and the whole mixture was stirred for 6 hours. Then the mixture was kept at room temperature until it cooled down. The resultant black solid was crushed and extracted with 20 ml aqueous NaOH (12%) solution and 20 ml dichloromethane (2–3 times) into a separating funnel. Then the organic layer was washed several times with water and dried over anhydrous Na_2SO_4, filtered and concentrated under reduced pressure. The final product was purified by silica gel chromatography. After purification the compounds were characterized *via* ^{1}H-NMR, FTIR, PXRD, DSC (Differential Scanning Calorimetry) [Fig. S1–S4†] and Single Crystal X-ray Diffraction (SCXRD).

Crystal growth and data collection

All the single crystals were obtained by the method of solvent evaporation at a slow rate. The synthesized compound was dissolved in a polar/non-polar solvent (HPLC grade) and then allowed to stand at different temperatures until the solvent had completely evaporated. The crystals of **DB10**, **DB11** and **DB23** were obtained from dichloromethane and hexane (4 : 1) solvent using a layering method at 5 °C. The crystal of **DB33** was obtained from toluene solvent at 25 °C. The single crystal diffraction data were collected on a Bruker APEX II diffractometer equipped with a CCD area detector using monochromated Mo Kα radiation using Bruker Apex II software.[39] The frames were integrated by using the Bruker SAINT[40] suite of programs. The crystal structures were solved by direct methods using the SIR 92 program.[41] The data were corrected for absorption effects using SADABS.[42] The structures were refined by the full matrix least squares method using SHELXL 2014[43] present in the program suite WinGX (version 2014.1).[44] The non-hydrogen atoms were refined anisotropically and the hydrogen atoms bonded to C and N atoms were positioned geometrically and refined using a riding model with U_{iso}(H) = 1.2U_{eq} (C, N). The crystal packing diagrams were generated using the Mercury 3.5.1 (CCDC) program.[45] Geometrical calculations were done using the programs PARST[46] and PLATON.[47] Table 1 lists the details of the structure refinement for the four new crystal structures.

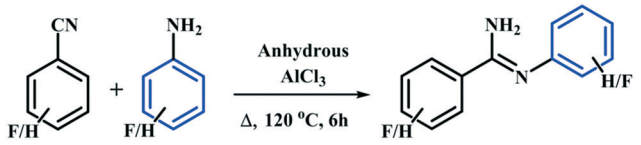

Scheme 1

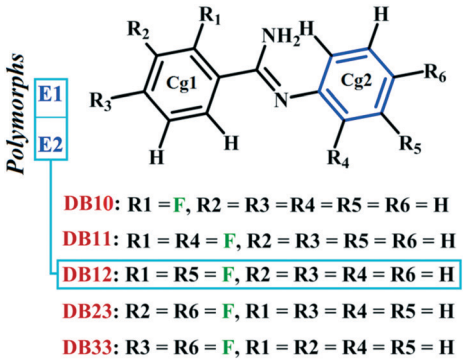

Scheme 2

Crystallographic modelling of disorder

The occupancies of the disordered fluorine atom (connected with the carbon atom in the *ortho* and *meta* positions on the phenyl ring) at two positions were refined by using the PART command in SHELXL 2014, namely F1A and F1B and F2A and F2B (the 'A' part contains the higher occupancy and the 'B' part contains the lower occupancy for that atom). The anisotropic displacement parameter for these two sites was fixed using the EADP command. The disorder of the phenyl rings was modelled using the AFIX 66 command for **DB11**. The C–F bond distances were fixed using the DFIX command in the case of **DB11** and **DB23**. Furthermore, the DFIX and FLAT commands were used to bring the minor part (F1B or F2B) of the fluorine atom in the plane (C1B > C6B) of the phenyl ring.

The previously investigated *E* isomer, in a similar class of compounds, **DB12** [(*E*)-2-fluoro-*N*′-(3-phenyl) benzimidamide][48] has two polymorphic forms, namely **E1** (form **I**) and **E2** (form **II**) wherein the role of N–H···π induced *E*/*Z* isomerization has been studied. Fig. S5† shows the ORTEPs for all the six compounds. It is noteworthy that **DB10** (*E*-isomer) is isostructural with the polymorphic form **E1** (refcode: KUCSOS) and **DB11** (*E*-isomer) is isostructural with the other polymorphic form **E2** (refcode: KUCZAL). Furthermore, another similar class of compound, **DB23** (*Z*-isomer), is isostructural with **DB33** (*Z*-isomer).

Computational analysis

XPac analysis

The crystal packing similarities which exist between these compounds (**DB10–E1**, **DB11–E2** and **DB23–DB33**) have been

Table 1 Data collection and details of the structure refinement

Sample code	DB10	DB11	DB23	DB33
Formula	$C_{13}H_{11}N_2F_1$	$C_{13}H_{10}N_2F_2$	$C_{13}H_{10}N_2F_2$	$C_{13}H_{10}N_2F_2$
Formula weight	214.24	232.23	232.23	232.23
Temperature (K)	100(2)	100(2)	100(2)	100(2)
Wavelength (Å)	0.71073	0.71073	0.71073	0.71073
Solvent system	DCM + hexane, LT	DCM + hexane, LT	DCM + hexane, LT	Toluene, RT
CCDC/refcode	982077	982078	982081	982085
Crystal system	Monoclinic	Monoclinic	Monoclinic	Monoclinic
Space group	$P2_1/c$	$C2/c$	$P2_1/c$	$P2_1/c$
a (Å)	12.5078(9)	22.9004(12)	9.4875(3)	9.6935(3)
b (Å)	8.3906(6)	11.9080(6)	11.5929(4)	10.9094(3)
c (Å)	11.3259(9)	8.2228(5)	10.3365(3)	10.3672(3)
α (°)	90.00	90	90	90
β (°)	116.232(4)	104.178(3)	93.915(2)	94.576(2)
γ (°)	90.00	90	90	90
V (Å^3)	1066.21(14)	2174.0(2)	1134.23(6)	1092.84(6)
Z', Z	1, 4	1, 8	1, 4	1, 4
Density (g cm^{-3})	1.335	1.419	1.360	1.411
μ (mm^{-1})	0.093	0.110	0.105	0.109
F (000)	448	960	480	480
θ (min, max)	1.82, 27.46	1.83, 30.16	2.15, 31.47	2.11, 27.39
Treatment of hydrogens	Fixed	Fixed	Fixed	Fixed
$h_{min,max}$, $k_{min,max}$, $l_{min,max}$	(−16, 16), (−7, 10), (−14, 14)	(−32, 32), (−16, 16), (−8, 11)	(−13, 11), (−12, 17), (−15, 15)	(−10, 12), (−9, 14), (−13, 13)
No. of ref.	8359	11 982	14 067	8976
No. of unique ref./obs. ref.	2361, 1727	3220, 2579	3696, 2804	2452, 2163
No. parameters	150	96	158	154
R_all, R_obs	0.0731, 0.0494	0.1010, 0.0850	0.0753, 0.0574	0.0433, 0.0380
wR_2_all, wR_2_obs	0.1388, 0.1250	0.2268, 0.2131	0.1511, 0.1413	0.1003, 0.0966
$\Delta\rho_{min,max}$ (e Å^{-3})	−0.401, 0.272	−0.996, 1.269	−0.582, 0.856	−0.231, 0.249
G. o. F.	1.072	1.107	1.073	1.040

analyzed quantitatively using the XPac 2.0.2[49,50] program. It gives information about the extent of dissimilarity (dissimilarity index x) as well as the dissimilarity parameters (stretch parameter, change in angles and planes) between two crystal structures. For XPac analysis, we have taken all the atomic coordinates (in crystal geometry) except for the hydrogen and fluorine atoms.

Intermolecular interaction energy

The dimeric interaction energies associated with the various non-covalent interactions present in the crystal packing were estimated using the PIXEL (version 12.5.2014)[51–57] program. The electron densities were calculated using the Gaussian 09 program[58] at the MP2/6-31G** level to generate the required PIXEL input. The total lattice energy of the molecule is classified into the corresponding Coulombic, polarization, dispersion and repulsion terms. In this study, all the analysis has been performed by taking the atomic coordinates of the major conformer A.

Energy vector model

The crystal packing similarity of these sets of isostructural compounds was also analyzed in terms of the energy vector model[59–61] using the *processPIXEL* method.[62] This constitutes a diagrammatic representation of the distribution of intermolecular interaction energies which govern the formation of supramolecular architectures.[62] The energy vector diagram represents the image of a molecule based on the energetic contribution (Coulombic, polarization, dispersion and repulsion) of each basic structural motif (BSM) related to the various symmetry operations in the crystal lattice. The vector length scaled against the total PIXEL energy for the corresponding pairwise intermolecular interactions is represented as:

$$L_i = (R_i E_i)/2E_{max} \quad (1)$$

where L_i is the scaled vector length for an interaction i, R_i is the distance between the molecular centers, E_i is the calculated interaction energy, and E_{max} is the most stabilizing calculated interaction energy in the structure.[63] From eqn (1), the vector corresponding to the most stabilizing molecular fragment has a length equal to half of the centroid–centroid distance between two interacting fragments and the most stabilizing pair is highlighted by a continuous line joining the centroids of the interacting molecules.

QTAIM analysis

Furthermore, QTAIM[64,65] analysis of some selected building blocks at the crystal geometry (with the hydrogen atoms moved to their neutron value) was performed at the MP2/6-311++G** level using the Gaussian 09 program. The formatted checkpoint file (fchk) was taken as the input file for AIMALL (version 13.05.06)[66] calculation. The topological features at the bond critical points are computed: (i) electron density (ρ_b), (ii) Laplacian ($\nabla^2\rho_b$), (iii) local potential energy (V_b), and (iv) kinetic energy density (G_b). The dissociation energies for the different intermolecular interactions were determined using the empirical approach: (i) $E_{int} = -0.5V_b$ (in au).[67,68]

Results and discussion

Analysis of structural similarity

Table S1† lists the three relevant torsions and the angle between the two phenyl rings at the crystal geometry. The torsion angles of these structures show that the molecular conformations of **DB10–E1** and **DB11–E2** are similar, whereas the molecular conformations of **DB23** and **DB33** are different and the dihedral angle between the two phenyl rings is 56.6° in **DB23** and 87.2° in **DB33**. XPac analysis shows that the isostructural compounds consist of three-dimensional (3D) supramolecular constructs with a dissimilarity index of 2.1 for **DB10–E1** (Fig. 1), 2.2 for **DB11–E2** (Fig. 2) and 9.7 for **DB23–DB33** (Fig. 3). The δ_p/δ_a [where δ_a and δ_p are the angular

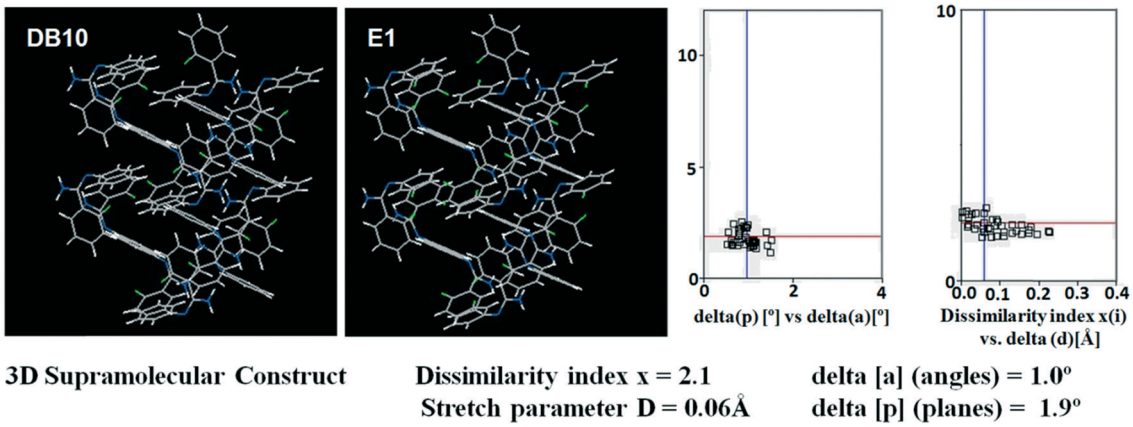

Fig. 1 3D supramolecular constructs obtained from XPac analysis of the isostructural molecules **DB10** and **E1**.

parameters for the change in angle and plane, respectively] diagrams for all the cases (**DB11–E1**, **DB11–E2** and **DB23–DB33**) contain a region with closely distributed data points at a low angle (δ_a = 1.0°, 1.6° and 3.6°). Similarly, X/δ_p diagrams which display the extent of stretching in the crystal packing of one structure compared to the other also show very closely distributed data points with stretch parameter = 0.06 Å and 0.10 Å for **DB11–E1** and **DB11–E2**, respectively, whereas in the case of **DB23–DB33**, the distributed data points are relatively spread out, the stretch parameter being 0.18 Å. Thus, this analysis fully supports that the crystal packing arrangements of the two polymorphic forms **E1** and **E2** are individually similar to the molecular arrangements of **DB10** and **DB11**, respectively.

Isostructural DB10–E1

DB10 (Fig. S5a†) and **E1** (Fig. S5b:† polymorphic form of **DB12**) crystallize in the monoclinic system in the centrosymmetric $P2_1/c$ space group with four molecules in the unit cell (Z = 4). The difference between these two structures is that **E1** has one extra fluorine atom attached at the *meta* position on the second phenyl ring (Cg2). The fluorine atom attached at the *ortho* position is positionally disordered and refined as F1A (major) and F1B (minor), F2A and F2B. Fig. 4 shows the overall molecular arrangement of (a) **DB10** and (b) **E1** down the *ab* plane. Table S2† lists the lattice energy of four new structures (**DB10**, **DB11**, **DB23** and **DB33**). All the molecular pairs were extracted from the crystal packing and their stabilization energies were obtained using the PIXEL method. Each molecular pair of one structure has an equivalent molecular pair [Fig. 5 and Fig. S6(a) and (b)†] associated with the same or different intermolecular interactions present in the crystal packing of compounds which exhibit isostructurality. The total stabilization energy for each molecular pair is partitioned into coulombic, polarization, dispersion and repulsion terms. Table 2 lists all the molecular pairs of **DB10** with their stabilization energies and the centroid–centroid distances. The molecular pairs of **E1** and **E2** were already mentioned (Table 2) in the previous report.[48] The primary building blocks (I; ~−42.5 kJ mol^{-1}) associated with the strong N–H···N ($d_{H\cdots N}$ = 2.11 Å and ∠N2–H2B···N1 = 149°) H-bonds and weak N–H···π ($d_{H\cdots Cg}$ = 2.36 Å and ∠N2–H2A···Cg1 = 161°) interactions generate a molecular chain along the crystallographic *b* axis. These molecular chains are interlinked with each other down the *ab* plane *via* weak C–H···F and C–H···π interactions and π···π stacking. Thus, the N–H···π interaction plays an important role in the observed isostructurality between **DB10** and **E1**. Fig. 6 shows the electrostatic and the dispersion contributions to the total

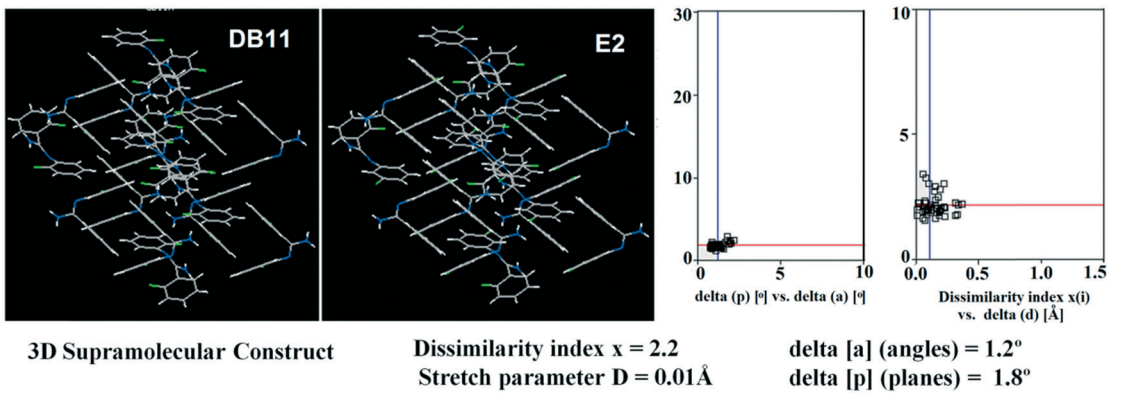

Fig. 2 3D supramolecular constructs obtained from XPac analysis of the isostructural molecules **DB11** and **E2**.

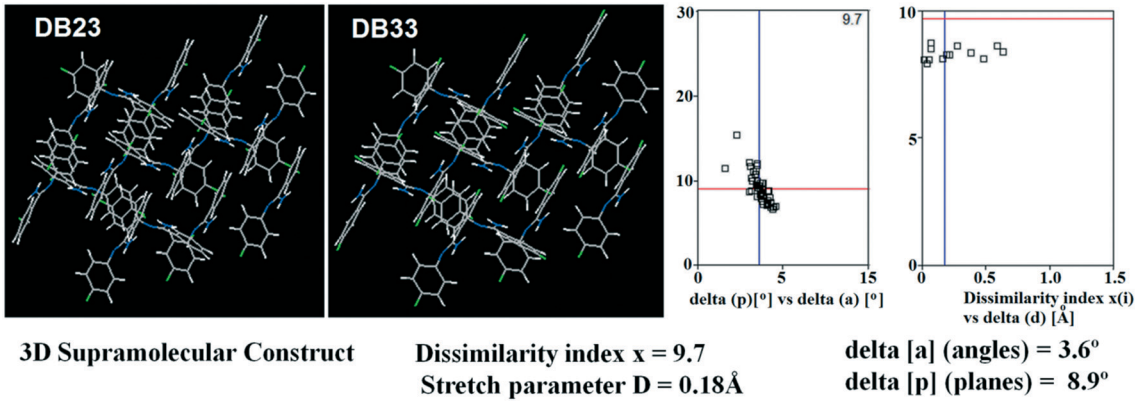

Fig. 3 3D supramolecular constructs obtained from XPac analysis of the isostructural molecules **DB23** and **DB33**.

stabilization for all the equivalent molecular pairs. In the case of the equivalent molecular pair **DB10–I** and **E1–I** (Fig. 5a), the electrostatic (64%) and the dispersion (36%) contributions to the total stabilization are comparable. The difference in the stabilization energies between the equivalent molecular pairs **DB10–III** (−21.2 kJ mol^{-1})/**E1–IV** (−19.3) (Fig. 5b) and **DB10–IV** (−19.9 kJ mol^{-1})/**E1–III** (−21.4 kJ mol^{-1}) (Fig. 5c) is −1.9 kJ mol^{-1}. Between the equivalent molecular pairs **DB10–IV**/**E1–III**, the latter has the intermolecular C–H···F interaction, but in the former case it is absent. Instead of a C–H···F interaction, there is the formation of a H···H contact with a distance of 2.35 Å (less than the sum of the vdW radii of hydrogen atoms). Because of this, **E1–III** has 6% more electrostatic contribution than **DB10–IV**. The equivalent molecular pairs **DB10–V**/**E1–V** (Fig. 5d) have a comparable energy of ∼−12.5 kJ mol^{-1}. Between the structurally equivalent molecular pairs **DB10–VI** (−12.2 kJ mol^{-1}) and **E1–VI** (−9.7 kJ mol^{-1}) (Fig. 5e), **E1–VI** has short C–H···F interactions ($d_{H\cdots F}$ = 2.40 Å) and a weak C–H···π interaction, but **DB10–VI** has only a weak C–H···π interaction. Thus, **DB10–VI** has 9% less electrostatic contribution compared to **E1–VI**. The equivalent molecular pairs **DB10–VII**/**E1–VII** (Fig. S6b†) and **DB10–VIII**/**E1–VIII** (Fig. 5f) also contribute to the stabilization of the crystal packing. The contributions from these molecular pairs are mainly of the dispersive (∼90%) type. In the case of the equivalent molecular pairs **DB10–II** (23.8 kJ mol^{-1}) and **E1–II** (25.9 kJ mol^{-1}) (case of parallel dipole···dipole interaction), the dispersion contribution is more dominant than the electrostatic contribution (Fig. S6a†). The centroid–centroid distances between two interacting molecules are 6.462 Å and 6.515 Å for **DB10–II** and **E1–II**, respectively. Hence the repulsion energy is less for **E1–II**.

Isostructural DB11–E2

The compounds **DB11** (Fig. S5c†) and **E2** (Fig. S5d†) crystallize in the centrosymmetric monoclinic space group *C*2/*c* with eight molecules in the unit cell (*Z* = 8). The difference between the two molecules is the change in fluorination on the second phenyl ring (Cg2), *i.e.* the fluorine atom is *ortho*-substituted for **DB11** and *meta*-substituted for **E2**. In each case, the fluorine atom is disordered over two positions, namely F1A (major part) and F1B (minor part); F2A and F2B. The crystal packing arrangements for **DB11** and **E2** are similar wherein for both cases the crystal packing is mainly stabilized *via* the centrosymmetric N–H···N dimer which

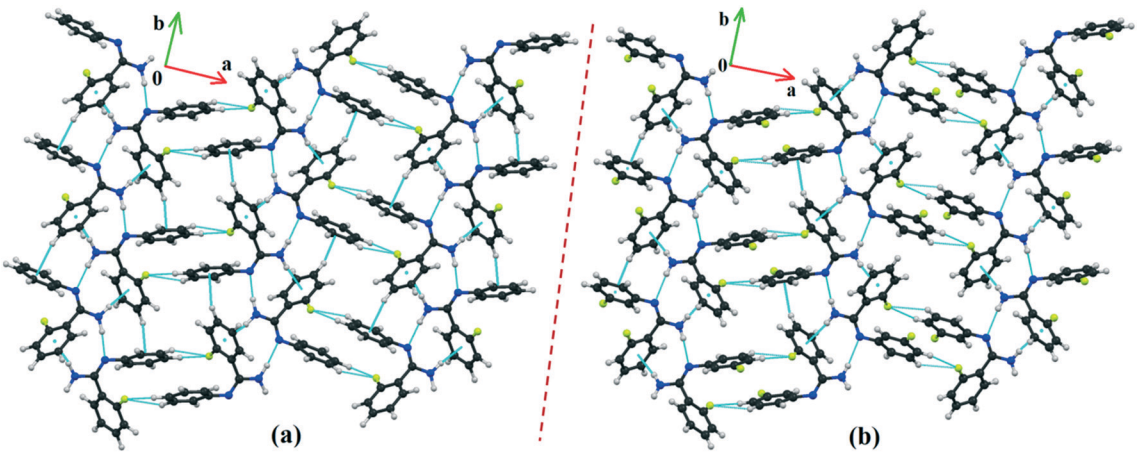

Fig. 4 The molecular arrangements of the isostructural compounds (a) **DB10** down the *ab* plane and (b) **E1** down the *ab* plane.

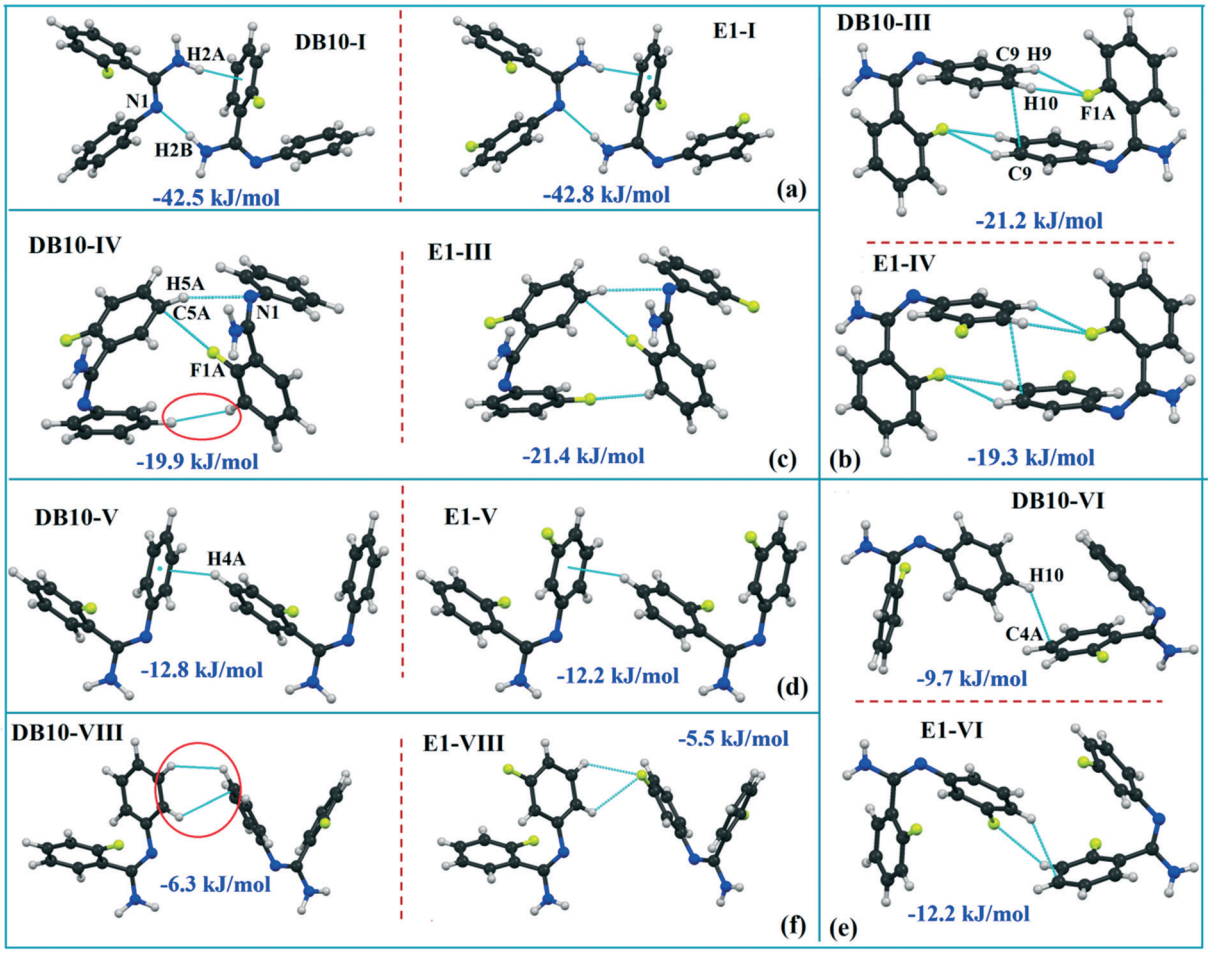

Fig. 5 The equivalent molecular building blocks (a–f) for the isostructural compounds **DB10**–**E1**.

plays a crucial role resulting in a similar packing pattern with structurally equivalent building blocks (Fig. 7). In the presence of a strong hydrogen bond, the synergistic effect of weak intermolecular interactions (like C–H···F, C–H···π and π···π

Table 2 The stabilization energy (in kJ mol^{-1}) of the molecular pairs for the **DB10** and **E1** [*D* = the centroid–centroid distance between two interacting molecules]

Motifs	Symmetry code	*D* (Å)	E_{Coul}	E_{Pol}	E_{Disp}	E_{Rep}	E_{Tot}	Possible interactions	Geometry (Å/°)
DB10									
I	$-x, y-1/2, -z+1/2$	7.086	−36.3	−18.6	−30.3	42.7	−42.5	N2–H2B···N1	2.11, 149
								N2–H2A···Cg1	2.36, 161
II	$-x, -y, 1-z$	6.462	−9.4	−1.8	−15.9	3.3	−23.8	vdWaals, C12–H12···N2	3.04, 143
								C6A–H6A···N1	3.28, 158
III	$1-x, -y, 1-z$	6.737	−6.1	−4.0	−32.2	21.1	−21.2	C10–H10···F1A	2.54, 122
								C9–H9···F1A	2.62, 119
								C9···C9	3.477(3)
IV	$x, -0.5-y, 0.5+z$	6.073	−6.6	−4.2	−29.5	20.5	−19.9	C5A–H5A···N1	2.59, 156
								C2A–F1A···C5A	2.988(3), 136
								H3A···H11	2.35
V	$x, 1+y, z$	8.391	−7.3	−4.0	−18.9	17.6	−12.8	C4A–H4A···Cg2	2.56, 136
VI	$1-x, -0.5+y, 1.5-z$	8.101	−1.3	−1.0	−12.0	4.6	−9.7	C10–H10···C4A	2.90, 136
VII	$-x, -1-y, 1-z$	8.862	1.1	−1.2	−13.5	6.5	−7.0	C5A···C6A	3.660(3)
VIII	$x, 0.5-y, 0.5+z$	8.396	−0.6	−0.8	−8.9	3.9	−6.3	H9···H11	2.70
								C8–H8···C11	2.99, 134
E1									
II	$2-x, -y, 1-z$	6.515	−12.1	−1.6	−14.0	1.8	−25.9	vdWaals, C12A–H12A···N2	3.44, 157
								C6A–H6A···N1	3.31, 142

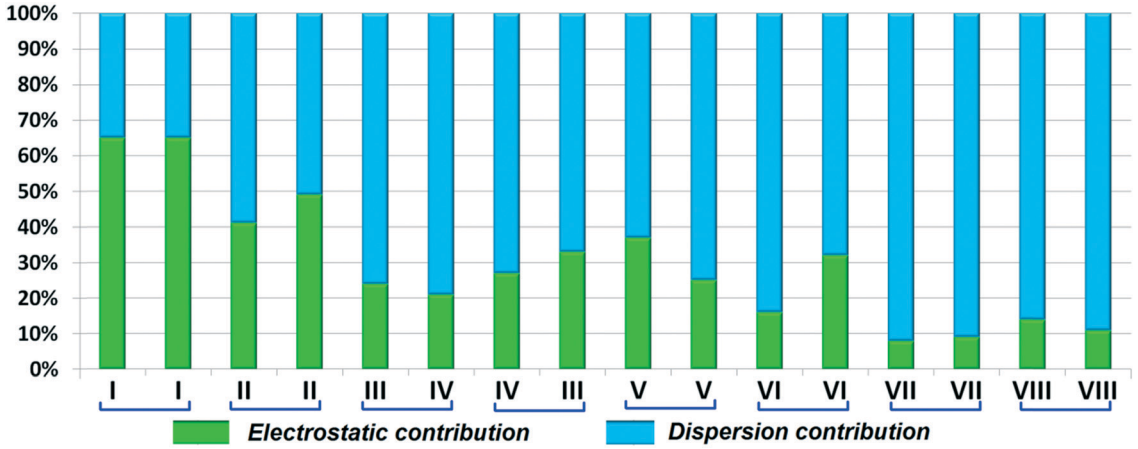

Fig. 6 Comparison of the percentage energy contribution towards total stabilization for the equivalent molecular pairs **DB10** and **E1**.

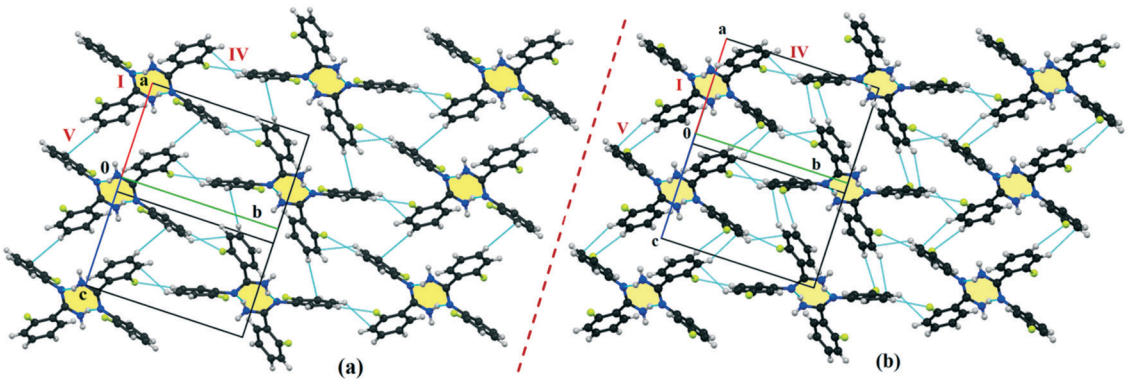

Fig. 7 The connectivity and the packing patterns for the isostructural (a) **DB11** and (b) **E2**.

Table 3 The stabilization energy (in kJ mol^{-1}) of the molecular pairs for **DB11** and **E2** [*D* = the centroid–centroid distance between two interacting molecules]

Motifs	Symmetry code	*D* (Å)	E_{Coul}	E_{Pol}	E_{Disp}	E_{Rep}	E_{Tot}	Possible interactions	Geometry (Å/°)
DB11									
I	$x, -y, 0.5 + z$	6.564	−30.7	−14.7	−36.7	40.0	−42.2	N2–H2B···N1	2.09, 156
								N2···C2A	3.563(4)
II	$2 - x, -y, 2 - z$	7.692	−32.1	−10.3	−17.9	19.9	−40.4	N2–H2A···N1	2.39, 144
III	$1.5 - x, 0.5 - y, 1 - z$	6.690	−9.7	−4.0	−30.8	18.3	−26.2	C4A–H4A···F2A	2.48, 154
								C4A···C5A	3.791(5)
IV	$x, 1 - y, 0.5 + z$	7.939	−4.2	−2.3	−16.2	10.3	−12.3	C9A–H9A···F1A	2.67, 138
V	$x, y, 1 + z$	8.223	−3.6	−1.7	−13.4	7.4	−11.4	C3A–H3A···π(C10A)	3.01, 143
VI	$1.5 - x, 0.5 - y, 2 - z$	7.645	−4.2	−1.4	−10.4	6.7	−9.3	C11A–H11A···F2A	2.49, 147
VII	$2 - x, 1 - y, 2 - z$	8.894	−1.4	−0.3	−7.0	1.4	−7.2	C9A–H9A···C8A	3.14, 138
VIII	$1.5 - x, 0.5 + y, 1.5 - z$	8.334	−0.8	−0.9	−9.0	3.9	−6.8	H11A···H6A	2.64
								H10A···H5A	2.40
IX	$2 - x, y, 1.5 - z$	5.684	2.4	−3.0	−27.7	28.1	−0.3	F1A···F1A	2.456(4)
								C8A–H8A···F1A	2.53, 123
E2									
III	$0.5 - x, 0.5 - y, 1 - z$	6.902	−7.4	−2.5	−22.3	8.4	−23.8	C4A–H4A···F2A	2.59, 128
								C4A···C5A	3.777(2)
VII	$1 - x, 1 - y, 2 - z$	8.685	−1.5	−0.2	−6.5	0.9	−7.3	C9A–H9A···C8A	3.60, 136

stacking) also provide additional stability to the crystal packing. From a detailed PIXEL analysis, all the molecular pairs were extracted from the crystal packing. Table 3 lists all the molecular pairs with their stabilization energies for **DB11**. The new molecular fragment **III** (centrosymmetric dimer associated with C–H···F interaction and π···π stacking) of **E2** is equivalent to the molecular fragment **III** of **DB11**. All the equivalent molecular pairs with their stabilization energies

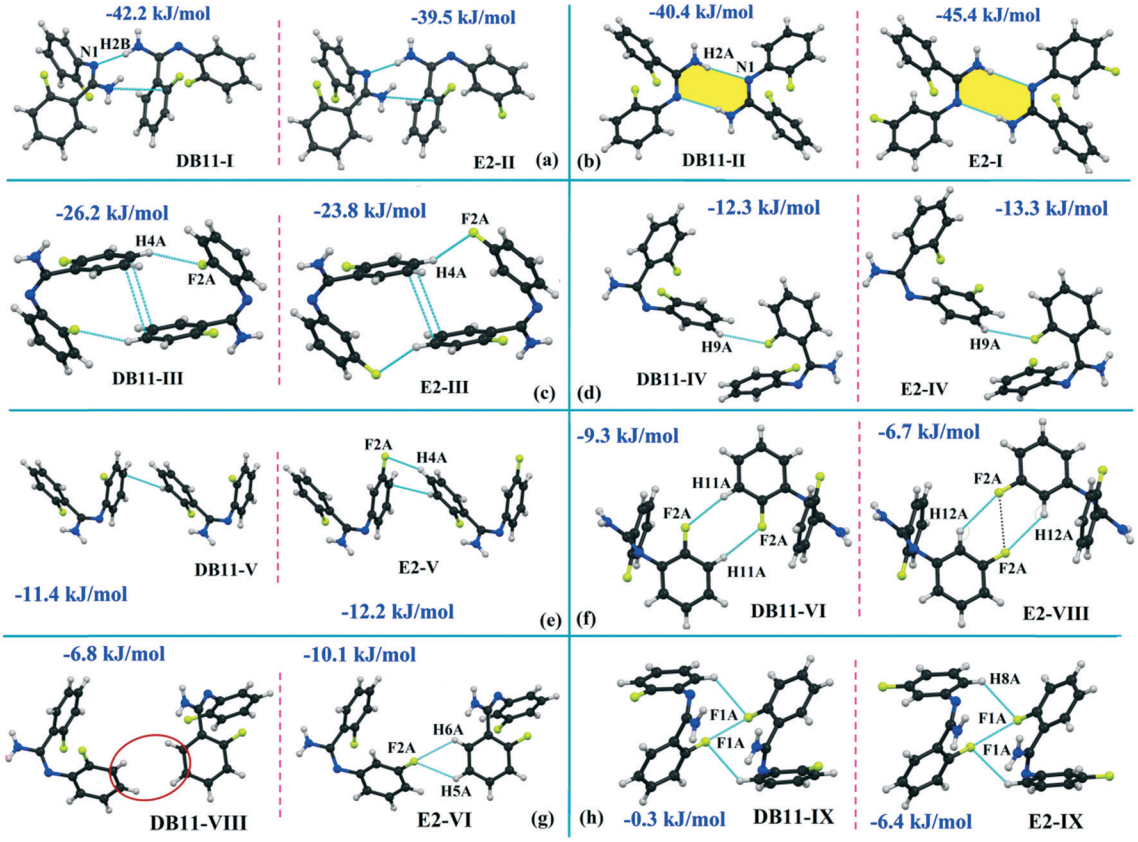

Fig. 8 The equivalent molecular building blocks (a–h) for the isostructural **DB11**–**E2**.

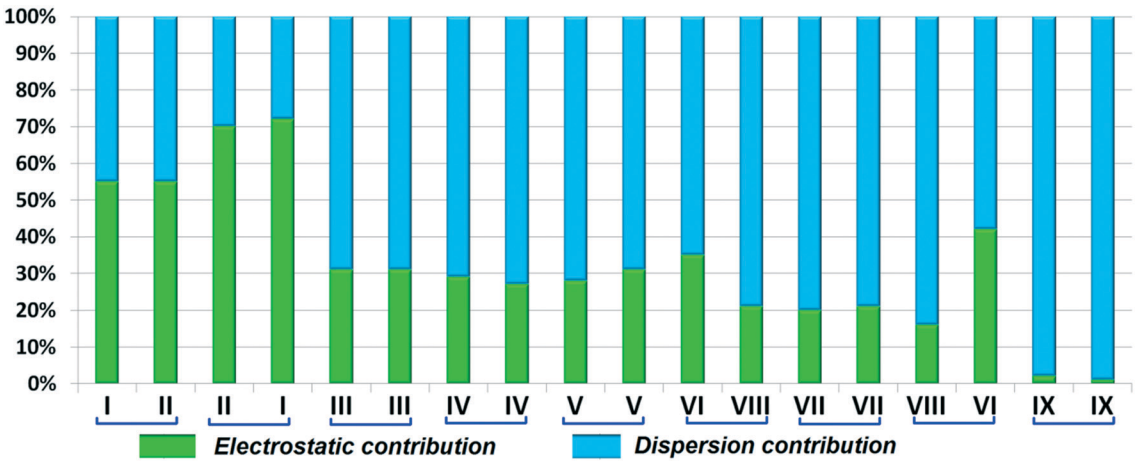

Fig. 9 Comparison of the percentage energy contribution towards the total stabilization of the equivalent molecular pairs for **DB11** and **E2**.

are shown in Fig. 8 and S6c.† In most of the equivalent motifs [a (**DB11–I** and **E2–II**), b (**DB11–II** and **E2–I**), c (**DB11–III** and **E2–III**), d (**DB11–IV** and **E2–IV**) and e (**DB11–V** and **E2–V**)] the stabilization energies are comparable with each other. Subsequently, the energetic contributions (electrostatic and dispersion contribution) are also equivalent (Fig. 9). The centrosymmetric N–H···N dimer is the strongest molecular pair (having a stabilization energy of −45.4 kJ mol^{-1}) for **E2** and provides maximum stability to the lattice, whereas **DB11–I** (involving a strong N–H···N hydrogen bond and a weak N···C contact) is the strongest molecular pair for **DB11**. In the case of the C–H···F centrosymmetric dimer [**DB11–VI** and **E2–VIII**; Fig. 8f] the stabilization energy is −2.6 kJ mol^{-1} higher for the former **DB11–VI** (which does not contain a F···F contact) than that for **E2–VII** [having a F···F contact, at a distance of 3.118(2) Å]. Furthermore, the electrostatic contribution is 12% more than

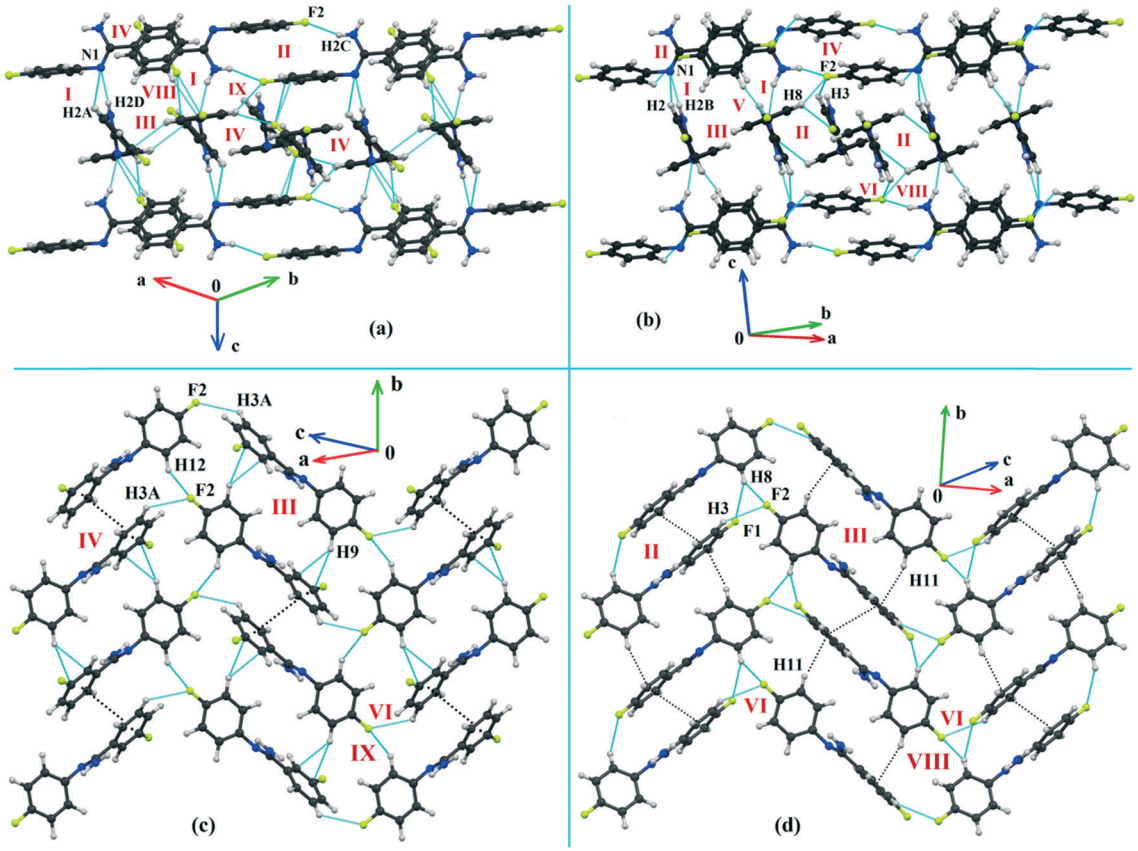

Fig. 10 The molecular arrangement of the isostructural compounds **DB23** [(a) and (c)] and **DB33** [(b) and (d)].

Table 4 The stabilization energy (in kJ mol^{-1}) of the molecular pairs for the isostructural molecules **DB23** and **DB33** [D = the centroid–centroid distance between two interacting molecules]

Motifs	Symmetry code	D (Å)	E_{Coul}	E_{Pol}	E_{Disp}	E_{Rep}	E_{Tot}	Possible interactions	Geometry (Å/°)
DB23									
I	x, 0.5 − y, 0.5 + z	5.272	−33.5	−15.1	−29.9	39.0	−39.5	N2–H2D···N1	2.05, 160
								C2A–H2A···N1	2.70, 133
II	−1 − x, 1 − y, 1 − z	9.198	−17.9	−5.2	−25.2	20.9	−27.3	N2–H2C···F2	2.19, 156
								C10(π)···C10(π)	3.367(2)
III	−x, 1 − y, 1 − z	5.138	−8.7	−3.9	−33.7	21.6	−24.7	C9–H9···π(C5A–C6A)	3.03, 158
IV	−x, −y, 1 − z	7.111	−7.3	−3.0	−30.3	16.1	−24.6	C2A···Cg1	3.550(2)
V	1 − x, −y, 1 − z	13.130	−5.5	−0.9	−6.5	3.0	−10.0	C4A–H4A···F1A	2.63, 177
VI	1 + x, 0.5 − y, 0.5 + z	10.541	−4.1	−1.2	−11.3	6.8	−9.9	C3A–H3A···F2	2.74, 116
VII	1 + x, y, z	9.488	−1.4	−0.8	−7.5	3.6	−6.0	C12–H12···F1A	2.57, 122
VIII	−x, 0.5 + y, 0.5 − z	7.419	−1.6	−1.2	−10.6	7.5	−5.9	F1A···π(C9–C10)	2.944(2)
IX	−1 − x, 0.5 + y, 0.5 − z	10.322	−1.2	−0.7	−5.2	2.7	−4.4	C12–H12···F2	2.52, 138
DB33									
I	x, 0.5 − y, 0.5 + z	5.230	−38.1	−17.0	−32.9	44.2	−43.8	N2–H2B···N1	2.09, 151
								C2–H2···N1	2.46, 162
II	1 − x, 1 − y, 2 − z	6.440	−10.2	−4.3	−43.2	28.4	−29.2	C8–H8···F1	2.56, 128
								Cg1···Cg1	3.738(2)
III	1 − x, −y, 2 − z	5.131	−12.7	−5.7	−40.0	30.5	−27.9	C11–H11···Cg1	2.81, 152
IV	−x, −y, 2 − z	9.303	−17.9	−5.8	−27.2	24.9	−26.0	N2–H2A···F2	2.20, 151
								π(C10)···π(C10)	3.261(2)
V	1 − x, −0.5 + y, 1.5 − z	7.313	−5.1	−3.2	−16.6	13.9	−11.0	C5–H5···Cg2	2.61, 143
VI	1 + x, 0.5 − y, 0.5 + z	10.644	−2.1	−1.3	−10.7	5.9	−8.2	C3–H3···F2	2.70, 135
VII	1 − x, 0.5 + y, 2.5 − z	8.192	1.0	−1.8	−8.9	4.3	−5.4	Dipole···dipole interaction	—
VIII	−x, 0.5 + y, 1.5 − z	10.280	−4.1	−1.6	−6.8	7.5	−5.0	C8–H8···F2	2.27, 146
IX	2 − x, 1 − y, 2 − z	13.007	−0.6	−0.3	−4.7	1.4	−4.2	F1···F1	2.984(1)

in the latter case. It is of interest to note that although **DB11–VIII** (−6.8 kJ mol^{-1}) and **E2–VI** (−10.1 kJ mol^{-1}), because of the existence of isostructurality, are the structurally equivalent motifs, following the robustness of the supramolecular

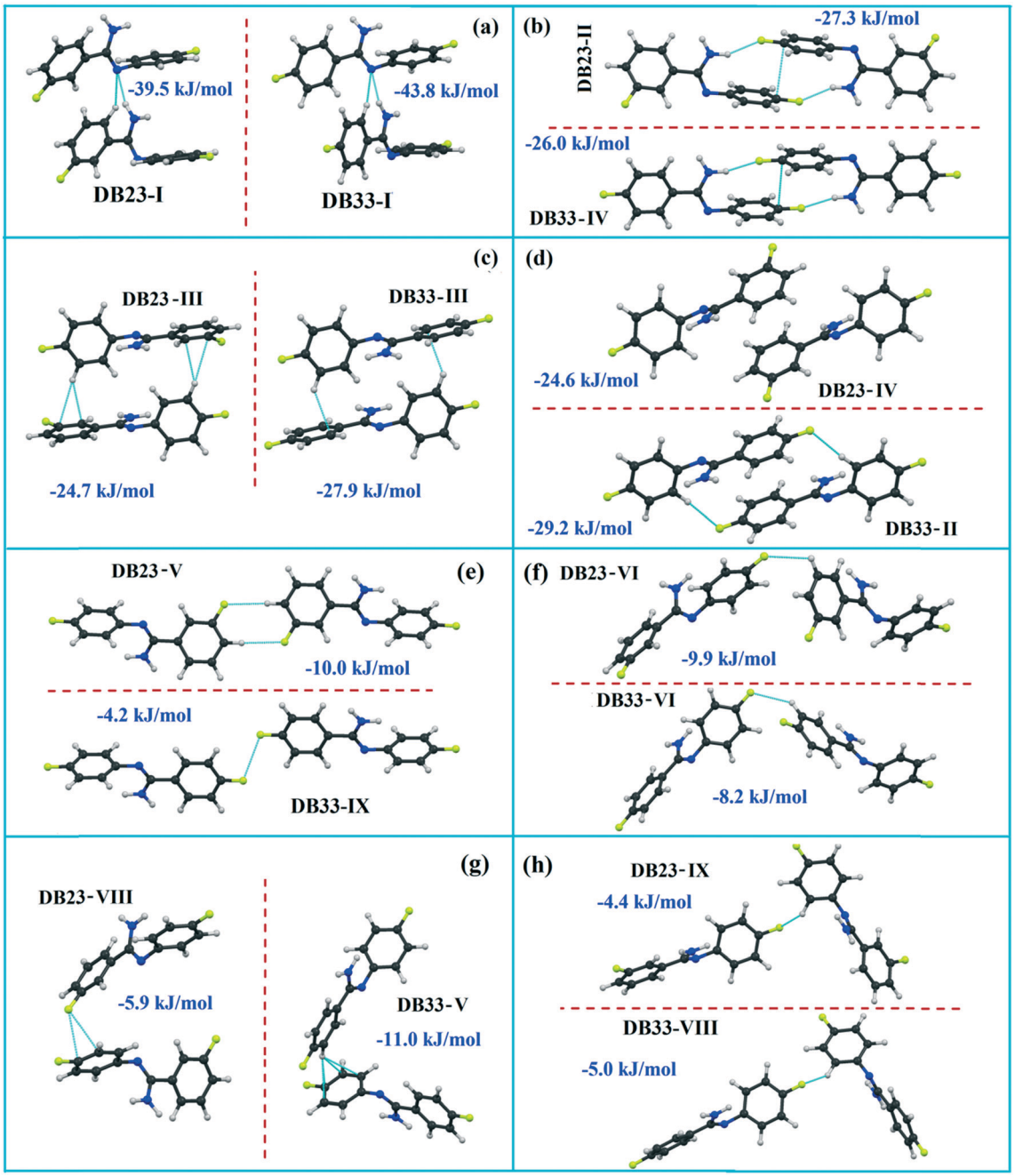

Fig. 11 The equivalent molecular building blocks (a–h) for the isostructural compounds **DB23**–**DB33**.

architecture (Fig. 8g), their stabilization energies are different. In **DB11–VIII**, as only a H···H contact is present, hence the maximum contribution comes from the dispersion (16% electrostatic) whereas in **E2–VI**, there is a formation of bifurcated C–H···F interactions (41% electrostatic). Between the molecular pairs **DB11–IX** (−0.3 kJ mol^{-1}; involving a short type I F1A···F1A contact with an "unusually short" distance of 2.456(4) Å) and **E2–IX** (−6.4 kJ mol^{-1}; involving a short type I F1A···F1A contact with a distance of 2.711(2) Å) [Fig. 8h], the electrostatic contribution is 13% more and the repulsion energy is 10.3 kJ mol^{-1} less in the case of **E2–IX** in comparison to the former.

Isostructural DB23–DB33

Both the compounds **DB23** (Fig. S5e†) and **DB33** (Fig. S5f†) crystallize in the centrosymmetric monoclinic $P2_1/c$ space group with closely related unit cell parameters having four molecules in the unit cell (Z' = 1, Z = 4). One fluorine atom is attached at the *para* position of the phenyl ring (Cg2) in both cases and the other fluorine atom is attached at the *meta* and *para* positions of the phenyl ring (Cg1) of **DB23** and **DB33**, respectively (Scheme 2). The molecular arrangements were stabilized *via* strong N–H···N chains (**DB23–I** and **DB33–I**; ~−42 kJ mol^{-1}) associated with the weak C–H···N interactions

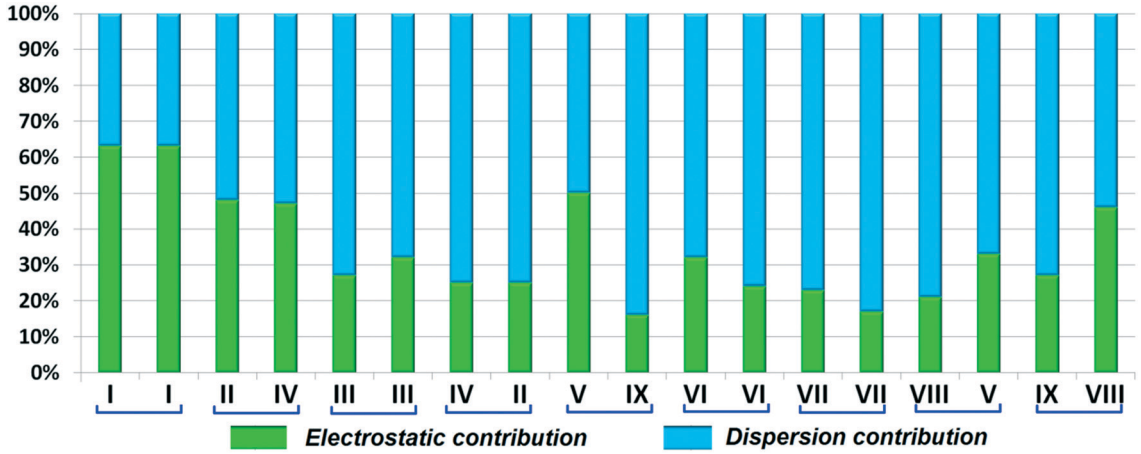

Fig. 12 Comparison of the percentage energy contribution towards total stabilization for the equivalent molecular pairs (**DB23** and **DB33**).

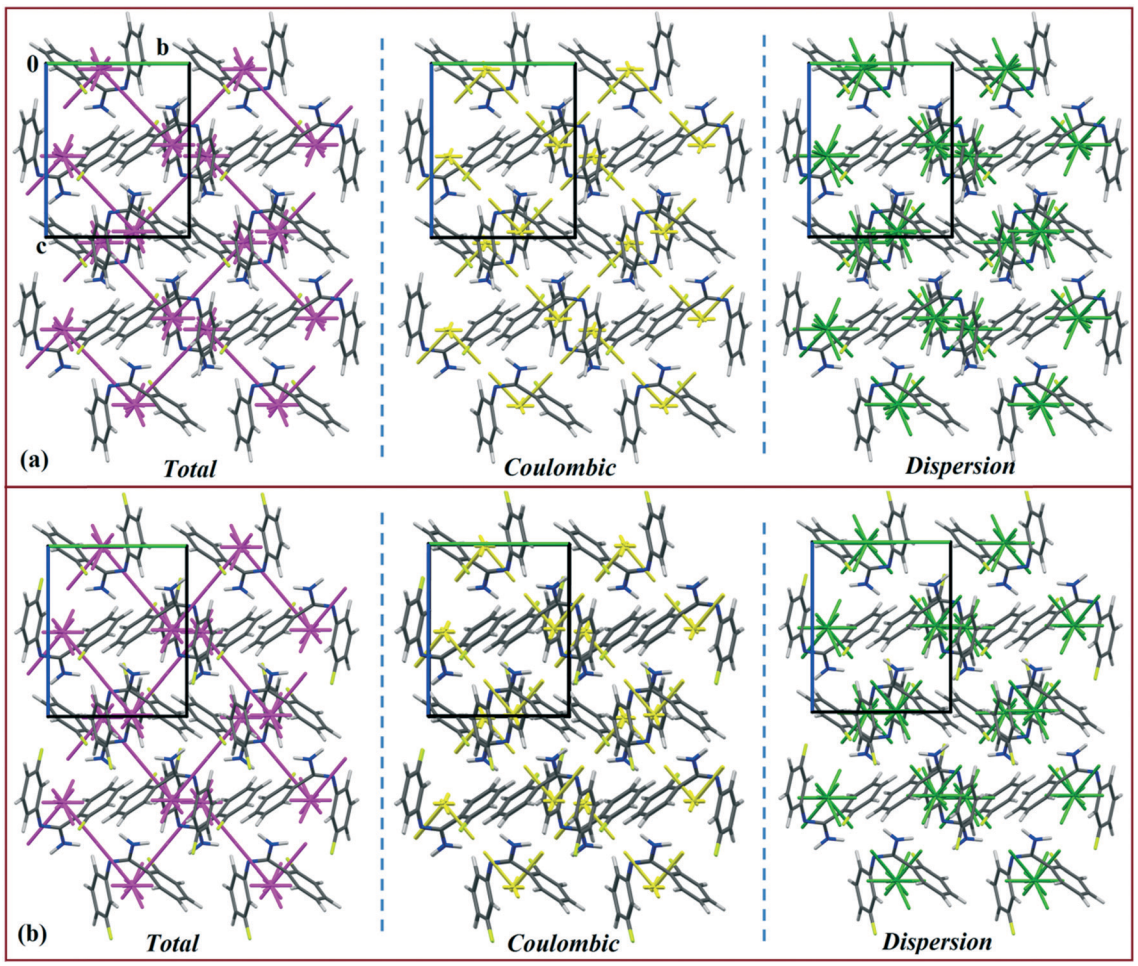

Fig. 13 Energy vector diagram for the isostructural (a) **DB10** and (b) **E1** down the *bc* plane.

along the *c* direction [Fig. 10(a) and (b)]. In addition, the weak intermolecular interactions like N–H···F, C–H···F, C–H···π and π···π also provide extra stability to the lattice. Table 4 lists the stabilization energy of each motif (extracted from the crystal packing) and the geometry of the interactions. All the equivalent structural motifs responsible for the formation of similar supramolecular architectures in isostructural **DB23** and **DB33** are shown in Fig. 11. Two parallel N–H···N chains were further connected with each other *via* a C–H···π intermolecular interaction (**DB23–III** and **DB33–III**) [Fig. 11c], the equivalent motif (**DB23–VIII** and **DB33–V**) [Fig. 11g], (**DB23–IV** and **DB33–II**) [Fig. 11d] and the

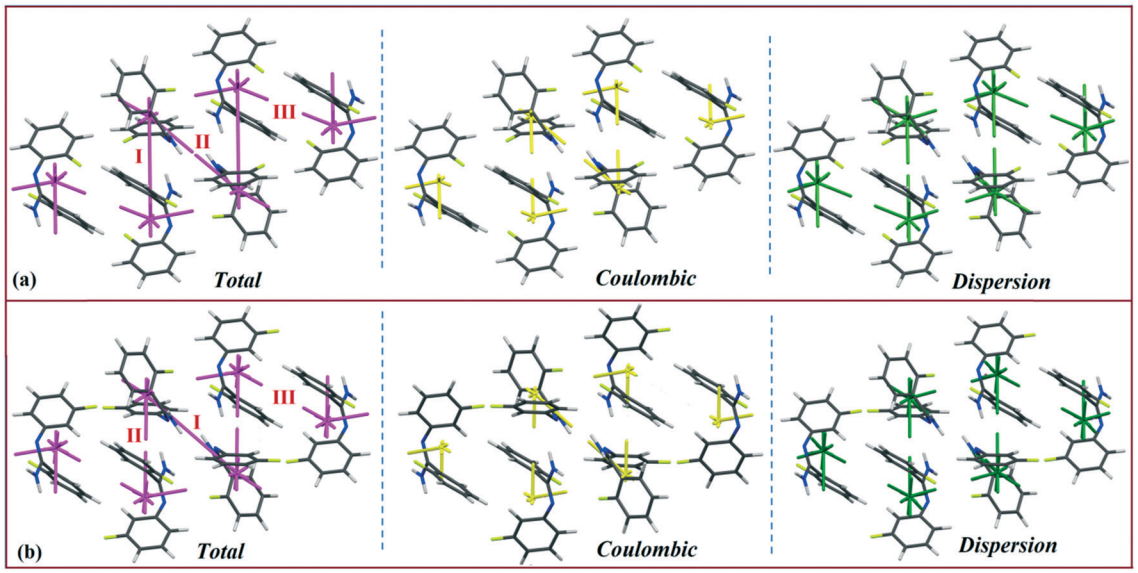

Fig. 14 Energy vector diagram for the isostructural (a) **DB11** (b) **E2** down the *ab* plane.

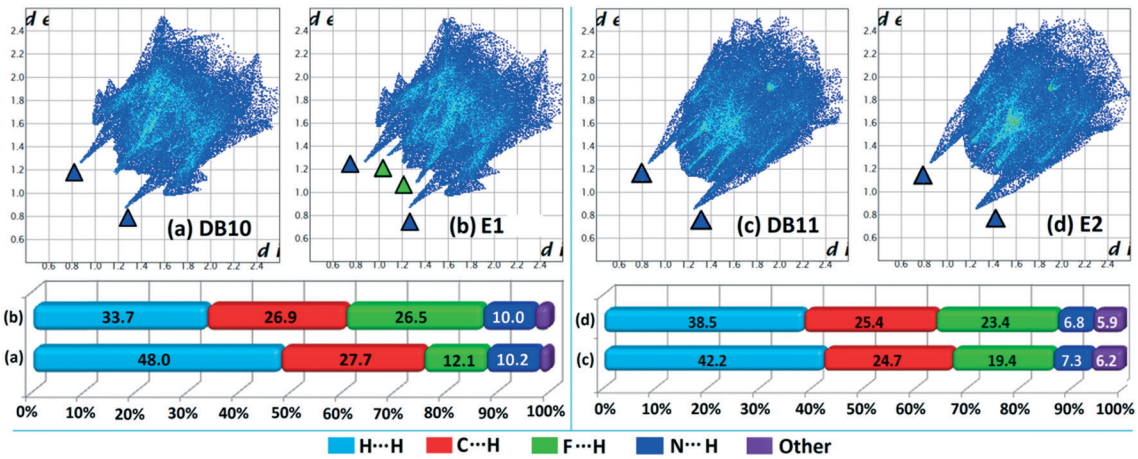

Fig. 15 The fingerprint plots and associated relative contribution of different atom···atom contacts in the crystal packing of isostructural compounds [(a) **DB10** and (b) **E1**; (c) **DB11** and (d) **E2**].

occurrence of a "short (2.20 Å) and highly directional (151°)" N–H···F dimer (**DB23–II** and **DB33–IV**) in the crystalline lattice which is further associated with π···π stacking [Fig. 10(a) and (b)]. On viewing down the *ab* plane the molecules form a zigzag array [Fig. 10(c) and (d)] associated with the molecular chains (involving weak C–H···F and C–H···π interactions) utilizing the structural building blocks **III**, **IV**, **VI** and **VII** for **DB23** and the motifs **II**, **III**, **VI** and **VIII** for **DB33** which provide additional stability to the crystal packing. From the overall molecular arrangements, considering that all the centroids of the phenyl ring of this array are combined together, leading to the formation of a distorted six-membered ring down the *ab* plane [Fig. 10(c) and (d)]. The four structurally equivalent molecular motifs (a), (b), (c) and (h) are also energetically equivalent but in the case of (c) (5% more electrostatic contribution for **DB33–III**) and (h) (17% more electrostatic contribution for **DB33–VIII**) the energetic contributions are not the same (Fig. 11 and 12). Between **DB23–IV** (−24.6 kJ mol^{-1}; having π···π stacking only) and **DB33–II** (−29.2 kJ mol^{-1}; associated with π···π stacking and C–H···F interaction) the electrostatic contribution is 8% more for **DB33–II** in comparison to the former (Fig. 11d). The centrosymmetric C–H···F dimeric motif **DB23–V** (−10.0 kJ mol^{-1}) is structurally (Fig. 11e) but not energetically equivalent to **DB33–IX** (−4.2 kJ mol^{-1}) having only a type I F···F contact with a distance of 2.984 (2) Å and subsequently the dispersion contribution is 36% more (Fig. 12) for **DB33–IX**.

Energy vector model

The energy vector models (magenta color) for **DB10–E1** and **DB11–E2** are shown in Fig. 13 and 14, respectively. The Coulombic (yellow color) and dispersion (green color) components were also scaled against the interaction energy of the most stabilizing molecular pair. In the case of **DB10–E1**, there is a formation of a zigzag continuous line (magenta

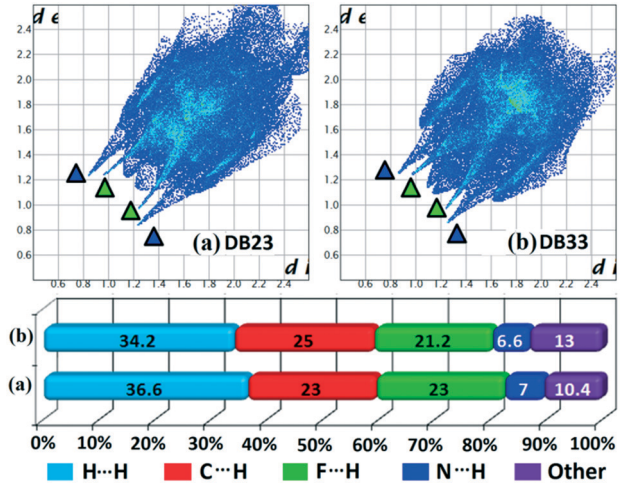

Fig. 16 The fingerprint plots and associated relative contribution of different atom···atom contacts in the crystal packing of isostructural compounds [(a) **DB23** and (b) **DB33**].

colored) between the two interacting fragments **I** (~−42 kJ mol^{-1}), whereas for the other interacting fragments, a discontinuous magenta colored line with a smaller gap (relatively more stabilizing) and a higher gap (relatively less stabilizing) appeared in both cases. Table S3† shows the energy vector lengths of some selected equivalent molecular pairs for the isostructural molecules. In the case of **DB11**, there is a continuous magenta colored line between the two interacting fragments **I** (−42.2 kJ mol^{-1}) and **II** (−40.4 kJ mol^{-1}) for **DB11**; **I** (−45.4 kJ mol^{-1}) and **II** (−39.5 kJ mol^{-1}) for **E2** having a comparable stabilization energy. Here, a discontinuous magenta colored line with a smaller gap and a higher gap is also observed for the other building blocks. The vector lengths (yellow color) for the coulombic component in molecular pairs I and II are longer than those of motif III whereas the vector lengths (green color) for the dispersion component in the molecular pair I and III are longer than those of motif III (Fig. 14a). In the case of **E2** (Fig. 14b), a similar feature was observed. Energy vector models for **DB23–DB33** are shown in Fig. S7.† In both cases, the strong N–H···N chain (**I**: more stabilizing) along the *c* axis leading to the formation of wave-like (magenta colored) columnar architectures is shown. Discontinuous lines (magenta colored) with less gap or higher gap were observed for other slightly less (**II**, **III**, **IV**) or more stabilizing molecular pairs. For **DB23**, the vector lengths for the Coulombic component (yellow color) in **I** and **II** are longer than those for the other motifs (Fig. S7a†), whereas the vector length for the dispersion component (green color) in **DB33–II** (Fig. S7b†) is longer than those of the other molecular fragments present in both **DB23–DB33**. Thus, according to the energy vector distribution patterns, **DB10** is isostructural with **E1**, **DB11** is isostructural with **E2**, and **DB23** is isostructural with the compound **DB33**.

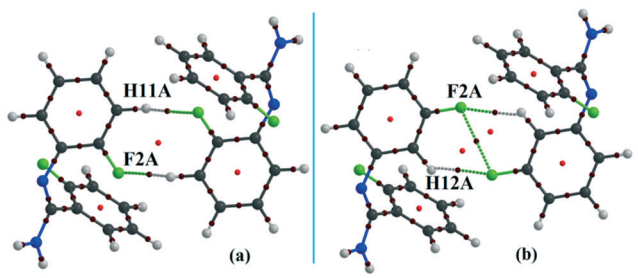

Fig. 17 Molecular graphs for the equivalent molecular pairs (a) **DB11–VI** and (b) **E2–VIII** associated with the C–H···F dimer [red color and deep red color depict the ring critical point and the bond critical point respectively].

Hirshfeld surface analysis

Hirshfeld surface analysis[69] was performed using CrystalExplorer 3.1[70] to further study the isostructurality behaviour between two sets of isostructural compounds, **DB10–E1** (Fig. 15a and b), **DB11–E2** (Fig. 15c and d) and **DB23–DB33** (Fig. 16), to account for the similarities in the crystal environment. Hirshfeld surface associated fingerprint plots[71,72] were analyzed to map the two-dimensional supramolecular blueprint to compare the three sets of isostructural compounds. The fingerprint plots and the relative contribution from the various atom···atom contacts are also shown. In the case of **DB10–E1** and **DB11–E2**, it is observed that both the fingerprint plots containing the sharp spikes (blue colored triangles) for the strong N–H···N hydrogen bond and the wing regions for the other contacts show the similarity in the packing patterns. Subsequently, the contributions from different atom···atom contacts are also comparable due to the closely related supramolecular architectures. The small spikes (green colored triangles) in **E2** signify the presence of short C–H···F interactions (**E2–V**) with a distance of 2.40 Å which is not observed in the fingerprint plot of **DB10**. In case of isostructural compounds **DB23** and **DB33**, two types of sharp spikes were observed. The spikes denoted with blue colored triangle correspond to the strong N–H···N hydrogen bonds and the spikes denoted with green colored triangle correspond to the presence of short N–H···F interactions. The atom···atom contributions for the different contacts are also similar to each other in three sets of isostructural compounds.

To obtain quantitative insights into the nature of various non-covalent interactions, QTAIM analysis was performed. In the ESI,† the molecular graphs for some selected building blocks (Fig. S8–S11†) for **DB10**, **DB11**, **DB23** and **DB33** are shown, where the bond critical points (3, −1) for the N–H···N, N–H···F, N–H···π, C–H···F, C–H···C, F···F interactions were obtained. The topological parameters [the electron density (ρ_{BCP}), the Laplacian ($\nabla^2\rho_{BCP}$), local potential energy (V_b), kinetic energy density (G_b) and the dissociation energy $DE^V(int)$ (= $-0.5V_b$)] for these BCPs are shown in Table S4.† The positive Laplacian values signify the closed shell interaction between the atoms. For the equivalent molecular motifs, the topological parameters are comparable. The electron density and the Laplacian value at the BCP for the intermolecular N–

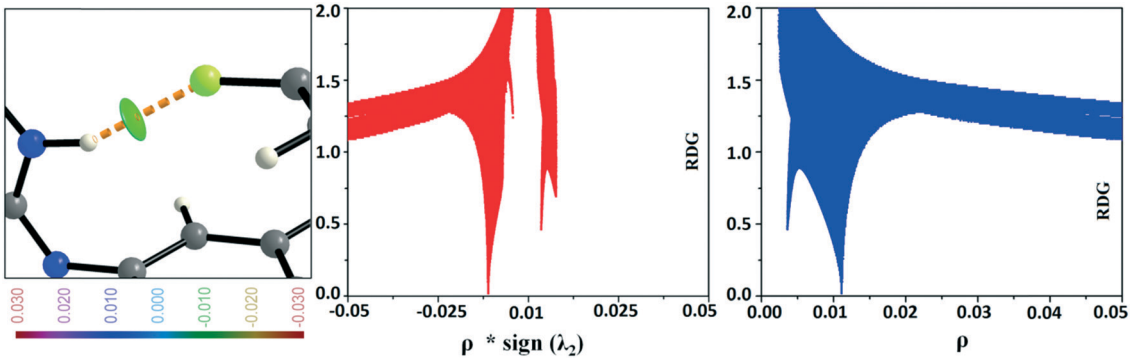

Fig. 18 RDG isosurface (s = 0.6) for the intermolecular N–H···F interaction and the plot of reduced density gradient (RDG) *versus* electron density multiplied by the sign of the second Hessian eigenvalue [$\rho \times$ sign (λ_2)] and electron density (ρ).

H···π interaction (**DB10**) are 0.0634 e Å^{-3} and 0.726 e Å^{-5}, respectively, which are comparable to the previously reported[48] values for **E1**. In the case of equivalent molecular pairs (f) (C–H···F dimer), for the isostructural **DB11–E2**, the molecular graphs are shown in Fig. 17. For **DB11–VI**, there is only one (3, +1) ring critical point whereas in **E2–VIII** there are two ring critical points due to the formation of a F···F contact. The electron density value at the BCP for the C–H···F interaction is observed to be 0.0475 e Å^{-3} for **DB11–VI** and 0.0316 e Å^{-3} for **E2–VIII** and the magnitude of the Laplacian is observed to be 0.723 e Å^{-5} for **DB11–VI** and 0.527 e Å^{-5} for **E2–VIII**. The corresponding bond dissociation energies are 6.7 kJ mol^{-1} and 4.1 kJ mol^{-1} for **DB11–VI** and **E2–VIII**, respectively. To get more insights into the nature of the C–H···F dimer, NCI (non-covalent index)[73,74] analysis was performed using the program NCImilano.[75,76] It is a graphical visualization of the regions where the non-covalent interactions take place.[77] The reduced density gradient (RDG) comes from the electron density (ρ) and its first derivative (gradient of the electron density):

$$s = \frac{1}{2\left(3\pi^2\right)^{1/3}} \frac{|\nabla\rho|}{\rho^{4/3}} \quad (2)$$

The reduced density gradient isosurface was generated at 0.6 (s) and plotted using MoleCoolQt[78] software. The NCI based RDG isosurface was plotted with the color range −0.03 $< \rho \times$ sign (λ_2) $<$ 0.03 au around the ring critical points and the bond critical points for the C–H···F dimeric motif in real space (Fig. S12†). RDG isosurface is based on the three components of the electron density distribution: electron density (ρ), reduced density gradient (RDG) and the gradient of the electron density ($\nabla\rho$). The sign of the second Hessian matrix indicates whether the intermolecular C–H···F is stabilized ($\lambda_2 < 0$) or destabilized ($\lambda_2 > 0$). In the case of **DB11–VI**, the RDG isosurface is light green colored (disc-shaped) having a negative eigenvalue ($\lambda_2 < 0$) around the BCP and shows the attractive nature of the C–H···F interaction. The 2D plots associated with the RDG *vs.* $\rho \times$ sign (λ_2) indicate a sharp spike in the negative region corresponding to the BCP and another sharp spike (for the dumb-bell shaped dodger blue RDG isosurface) in the positive region corresponding to the ring critical point. But in the case of **E2–VIII**, there is a total of three light sky blue RDG isosurfaces, *i.e.*, two disc-shaped which correspond to the BCP for the C–H···F interaction and the third one (dispersive nature) corresponds to the BCP for the F···F contact. Here the value of $\rho \times$ sign (λ_2) is less negative compared to the value for the C–H···F present in **DB11–VI**. In addition, there is a total of two dodger blue RDG isosurface regions which correspond to the two ring critical points in **E2–VIII**.

In the occurrence of the isostructurality for **DB23–DB33**, the intermolecular N–H···F interaction plays an important role in the presence of a strong N–H···N chain. This interaction is rarely observed in the formation of organic solids, containing the N–H or NH_2 functional group along with the C–F bond. Here, there is a formation of a centrosymmetric dimer utilizing the short and highly directional N–H···F

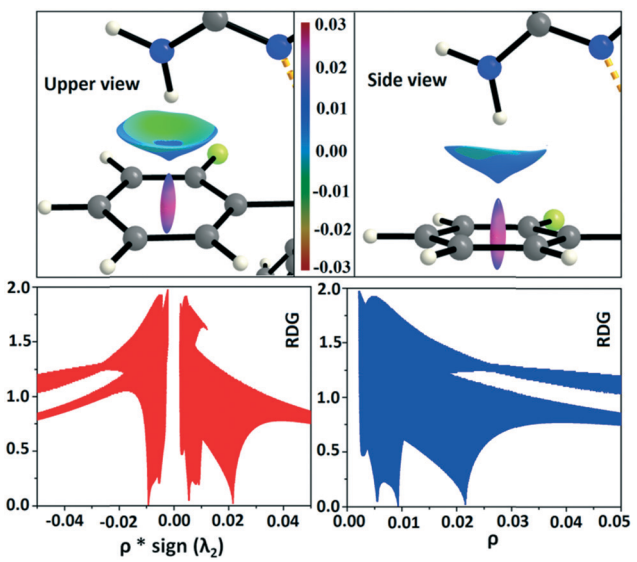

Fig. 19 RDG isosurface (s = 0.6) for intermolecular N–H···π interaction (**DB10–I**) and the plot of reduced density gradient (RDG) *versus* electron density multiplied by the sign of the second Hessian eigenvalue [$\rho \times$ sign (λ_2)] and electron density (ρ).

interaction. Cambridge Structural Database[79] (CSD: version 5.37) search has been performed taking the different constraints: $d_{H\cdots F}$ = 2.0 to 2.3 Å, ∠N–H···F = 140 to 180°, *R* factor ≤ 0.1, not disordered, not polymeric, no errors, no ions, no powder structures, and only organic compounds. A CSD study reveals that the total number of hits is 19 for the compounds having the NH_2 group (Fig. S13 and S14†). The NCI-based RDG isosurface for the N–H···F interaction also shows a green colored disc (Fig. 18) with a highly negative value (∼−0.0105 au) of $\rho \times$ sign (λ_2) which indicates the attractive (stabilized) nature of this type of interaction. Furthermore, the NCI analysis of the N–H···π (**DB10**) interaction gives some interesting information about the nature of this interaction. It shows that there is formation of a "funnel-like" RDG isosurface (Fig. 19) in which the inside surface color of the funnel is green (stabilized interaction), and the outside surface color is light blue (destabilized). In addition, there is also one small light blue colored (destabilized) region around the bond critical point. The pink colored RDG isosurface (vertical spike) formed around the ring critical point inside the phenyl ring indicates the more destabilized interaction.

Summary

In this study, the crystal structures of fluorine containing molecules, existing as *E–Z* isomers, are found to exhibit isostructurality, having equivalent supramolecular building blocks. Thus, the substitution at the fluorine atom on the phenyl ring is responsible for the observed isostructurality in isomeric fluorinated phenyl benzamidine compounds. Most of the structurally equivalent motifs present in the crystal packing are isoenergetic and the contribution of electrostatic and dispersion interactions is comparable in these compounds. The structural similarity analysis supports quantitatively the existence of isostructurality, and the NCI analysis establishes the N–H···F and N–H···π interactions to be "attractive" in nature. The energy distribution patterns for the energy vector models are similar in both sets of isostructural compounds. The Hirshfeld surface analysis also helps to verify the behaviour of isostructurality in terms of fingerprint plots associated with various non-covalent interactions in the crystal. This study once again illustrates the significance of weak and rare intermolecular interactions in the solid state and hence depict the pivotal point that the study and investigation of interactions in molecular crystals is an important exercise. This has special relevance and significance in the design of crystals with desired properties with implications in polymorphism, cocrystal formation, and the development of technologically important materials.

Acknowledgements

D. D. thanks IISER Bhopal for the research fellowship. D. C. and D. D. thank IISER Bhopal for the use of the research facilities and infrastructure, and SERB for research funding.

References

1 G. Bolla, S. Mittapalli and A. Nangia, *IUCrJ*, 2015, **2**, 389–401.
2 T. Steiner, *Angew. Chem., Int. Ed.*, 2002, **41**, 48–76.
3 J. M. Pollino and M. Weck, *Chem. Soc. Rev.*, 2005, **34**, 193–207.
4 G. R. Desiraju, *Crystal Engineering: the Design of Organic Solids*, Amsterdam, Elsevier, 1989.
5 IUCr, http://reference.iucr.org/dictionary/Isostructural_crystals, Accessed 18/11/2014.
6 D. Dey, S. P. Thomas, M. A. Spackman and D. Chopra, *Chem. Commun.*, 2016, **52**, 2141–2144.
7 K. Dziubek, M. Podsiadlo and A. Andrzej, *J. Am. Chem. Soc.*, 2007, **129**, 12620–12621.
8 L. Fabian and A. Kalman, *Acta Crystallogr., Sect. B: Struct. Sci., Cryst. Eng. Mater.*, 2004, **60**, 547–558.
9 T. Gelbrich, D. S. Hughes, M. B. Hursthouse and T. L. Threlfall, *CrystEngComm*, 2008, **10**, 1328–1334.
10 N. K. Nath, B. K. Saha and A. Nangia, *New J. Chem.*, 2008, **32**, 1693–1701.
11 R. Thakuria, N. K. Nath, S. Roy and A. Nangia, *CrystEngComm*, 2014, **16**, 4681–4690.
12 M. C. Pfrunder, A. S. Micallef, L. Rintoul, D. P. Arnold, K. J. P. Davy and J. McMurtrie, *Cryst. Growth Des.*, 2014, **14**, 6041–6047.
13 D. Cincic, T. Friscic and W. Jones, *New J. Chem.*, 2008, **32**, 1776–1781.
14 T. Hosokawa, S. Datta, A. R. Sheth, N. R. Brooks, V. G. Young and D. J. W. Grant, *Cryst. Growth Des.*, 2004, **4**, 1195–1201.
15 S. L. Childs, L. J. Chyall, J. T. Dunlap, V. N. Smolenskaya, B. C. Stahly and G. P. Stahly, *J. Am. Chem. Soc.*, 2004, **126**, 13335–13342.
16 A. V. Trask, D. A. Haynes, W. D. S. Motherwell and W. Jones, *Chem. Commun.*, 2006, 51–53.
17 A. V. Trask and W. Jones, *Top. Curr. Chem.*, 2005, **254**, 41–70.
18 A. V. Trask, W. D. S. Motherwell and W. Jones, *Chem. Commun.*, 2004, 890–891.
19 A. V. Trask, W. D. S. Motherwell and W. Jones, *Cryst. Growth Des.*, 2005, **5**, 1013–1021.
20 A. V. Trask, W. D. S. Motherwell and W. Jones, *Int. J. Pharm.*, 2006, **320**, 114–123.
21 S. Ebenezer, P. T. Muthiah and R. J. Butcher, *Cryst. Growth Des.*, 2011, **11**, 3579–3592.
22 C. Capacci-Daniel, S. Dehghan, V. M. Wurster, J. A. Basile, R. Hiremath, A. A. Sarjeantb and J. A. Swift, *CrystEngComm*, 2008, **10**, 1875–1880.
23 T. Gelbrich, T. L. Threlfall and M. B. Hursthouse, *CrystEngComm*, 2012, **14**, 5454–5464.
24 S. J. Coles, T. L. Threlfall and G. J. Tizzard, *Cryst. Growth Des.*, 2014, **14**, 1623.
25 A. Kalman, S. Parkanyi and G. Argay, *Acta Crystallogr., Sect. B: Struct. Sci.*, 1993, **49**, 1039–1049.
26 W. Szczepankiewicz, J. Suwinski and Z. Karczmarzyk, *Chem. Heterocycl. Compd.*, 2004, **40**, 801.

27 A. Schmidpeter, R. K. Bansal, K. Karaghiosoff, F. Steinmuller and C. Spindler, *Phosphorus, Sulfur Silicon Relat. Elem.*, 1990, **49/50**, 349.
28 L. Capuano, W. Fischer, H. Scheidt and M. Schneider, *Chem. Ber.*, 1978, **111**, 2497.
29 Y. G. Shermolovich, V. S. Talanov, V. V. Pirozhenko and L. N. Markovskii, *Russ. J. Org. Chem.*, 1982, **18**, 2240.
30 T. Asano, T. Yoshikawa, H. Nakamura, Y. Uehara and Y. Yamamoto, *Bioorg. Med. Chem. Lett.*, 2004, **14**, 2299–2302.
31 T. Asano, T. Yoshikawa, T. Usui, H. Yamamoto, Y. Yamamoto, Y. Uehara and H. Nakamura, *Bioorg. Med. Chem.*, 2004, **12**, 3529–3542.
32 H. Nakamura, Y. Sasaki, M. Uno, T. Yoshikawa, T. Asano, H. S. Ban, H. Fu-kazawa, M. Shibuya and Y. Uehara, *Bioorg. Med. Chem. Lett.*, 2006, **16**, 5127–5131.
33 P. A. Koutentis and S. I. Mirallai, *Tetrahedron*, 2010, **66**, 5134–5139.
34 I. Ojima, *Fluorine in Medicinal Chemistry and Chemical Biology*, Wiley- Blackwell, Chichester, West Sussex, PO19 8SQ, UK, 2009.
35 V. Gouverneur and K. Seppelt, *Chem. Rev.*, 2015, **115**, 563–565.
36 C. Isanbor and D. O'Hagan, *J. Fluorine Chem.*, 2006, **127**, 303–319.
37 I. Ojima, *J. Org. Chem.*, 2013, **78**, 6358–6383.
38 P. Panini and D. Chopra, *Cryst. Growth Des.*, 2014, **14**, 3155–3168.
39 *Apex2*, Version 2 User Manual, M86-E01078, Bruker Analytical X-ray Systems, Madison, WI, 2006.
40 *Siemens, SMART System*, Siemens Analytical X-ray Instruments Inc., Madison, MI, 1995.
41 A. Altomare, M. C. Burla, G. Camalli, G. Cascarano, C. Giacovazzo, A. Gualiardi and G. Polidori, *J. Appl. Crystallogr.*, 1994, **27**, 435–436.
42 G. M. Sheldrick, *SADABS*, Bruker AXS, Inc., Madison, WI, 2007.
43 L. J. Farrugia, *J. Appl. Crystallogr.*, 1999, **32**, 837–838.
44 G. M. Sheldrick, *Acta Crystallogr., Sect. A: Found. Crystallogr.*, 2008, **64**, 112–122.
45 C. F. Macrae, I. J. Bruno, J. A. Chisholm, P. R. Edgington, P. McCabe, E. Pidcock, L. Rodriguez-Monge, R. Taylor, J. Streek and P. A. Wood, *J. Appl. Crystallogr.*, 2008, **41**, 466–470.
46 M. Nardelli, *J. Appl. Crystallogr.*, 1995, **28**, 659.
47 A. L. Spek, *Acta Crystallogr., Sect. D: Biol. Crystallogr.*, 2009, **65**, 148–155.
48 D. Dey and D. Chopra, *CrystEngComm*, 2015, **17**, 5288–5298.
49 T. Gelbrich and M. B. Hursthouse, *CrystEngComm*, 2006, **8**, 448–460.
50 F. P. A. Fabbiani, B. Dittrich, A. J. Florence, T. Gelbrich, M. B. Hursthouse, W. F. Kuhs, N. Shankland and H. Sowa, *CrystEngComm*, 2009, **11**, 1396–1406.
51 J. D. Dunitz and A. Gavezzotti, *Cryst. Growth Des.*, 2012, **12**, 5873–5877.
52 J. D. Dunitz and A. Gavezzotti, *Chem. Soc. Rev.*, 2009, **38**, 2622–2633.
53 J. D. Dunitz and A. Gavezzotti, *Angew. Chem., Int. Ed.*, 2005, **44**, 1766–1787.
54 A. Gavezzotti, *CrystEngComm*, 2003, **5**, 429–438.
55 L. Maschio, B. Civalleri, P. Ugliengo and A. Gavezzotti, *J. Phys. Chem. A*, 2011, **115**, 11179–11186.
56 J. D. Dunitz and A. Gavezzotti, *Cryst. Growth Des.*, 2005, **5**, 2180–2189.
57 L. Carlucci and A. Gavezzotti, *Chem. – Eur. J.*, 2005, **11**, 271–279.
58 M. J. Frisch, G. W. Trucks, H. B. Schlegel, G. E. Scuseria, M. A. Robb, J. R. Cheeseman, G. Scalmani, V. Barone, B. Mennucci, G. A. Petersson, H. Nakatsuji, M. Caricato, X. Li, H. P. Hratchian, A. F. Izmaylov, J. Bloino, G. Zheng, J. L. Sonnenberg, M. Hada, M. Ehara, K. Toyota, R. Fukuda, J. M. HasegawaIshida, T. Nakajima, Y. Honda, O. Kitao, H. Nakai, T. Vreven, J. A. Montgomery Jr., J. E. Peralta, F. Ogliaro, M. Bearpark, J. J. Heyd, E. Brothers, K. N. Kudin, V. N. Staroverov, R. Kobayashi, J. Normand, K. Raghavachari, A. Rendell, J. C. Burant, S. S. Iyengar, J. Tomasi, M. Cossi, N. Rega, J. M. Millam, M. Klene, J. E. Knox, J. B. Cross, V. Bakken, C. Adamo, J. Jaramillo, R. Gomperts, R. E. Stratmann, O. Yazyev, A. J. Austin, R. Cammi, C. Pomelli, J. W. Ochterski, R. L. Martin, K. Morokuma, V. G. Zakrzewski, G. A. Voth, P. Salvador, J. J. Dannenberg, S. Dapprich, A. D. Daniels, Ö. Farkas, J. B. Foresman, J. V. Ortiz, J. Cioslowski and D. J. Fox, *Gaussian 09*, Revision D.01, Gaussian, Inc., Wallingford, CT, 2009.
59 O. V. Shishkin, V. V. Dyakonenko, A. V. Maleev, D. Schollmeyer and M. O. Vysotsky, *CrystEngComm*, 2011, **13**, 800–805.
60 O. V. Shishkin, V. V. Medvediev, R. I. Zubatyuk, O. O. Shyshkina, N. V. Kovalenko and J. M. Volovenko, *CrystEngComm*, 2012, **14**, 8698–8707.
61 O. V. Shishkin, V. V. Medvedieva and R. I. Zubatyuka, *CrystEngComm*, 2013, **15**, 160–167.
62 A. D. Bond, *J. Appl. Crystallogr.*, 2014, **47**, 1777–1780.
63 O. V. Shishkin, V. V. Dyakonenko and A. V. Maleev, *CrystEngComm*, 2012, **14**, 1795–1804.
64 R. F. W. Bader, *Atoms in Molecules: A Quantum Theory*, Oxford University Press, Oxford, U.K., 1990.
65 V. G. Tsirelson, *The Quantum Theory of Atoms in Molecules: From Solid State to DNA and Drug Design*, ed. C. Matta and R. Boyd, Wiley-VCH, Weinheim, Germany, 2007, ch. 10, p. 45.
66 T. A. Keith, *AIMALL*, version 13.05.06, TK Gristmill Software, Overland Park KS, 2013, aim.tkgristmill.com.
67 I. Mata, I. Alkorta, E. Espinosa and E. Molins, *Chem. Phys. Lett.*, 2011, **507**, 185–189.
68 E. Espinosa, E. Molins and C. Lecomte, *Chem. Phys. Lett.*, 1998, **285**, 170–173.
69 M. A. Spackman and D. Jayatilaka, *CrystEngComm*, 2009, **11**, 19–32.
70 S. K. Wolff, D. J. Grimwood, J. J. McKinnon, M. J. Turner, D. Jayatilaka and M. A. Spackman, *CrystalExplorer, Version 3.1*, University of Western Australia, Crawley, Australia, 2012.

71 M. A. Spackman and J. J. Mckinnon, *CrystEngComm*, 2002, **4**, 378–392.
72 J. J. Mckinnon, D. Jayatilaka and M. A. Spackman, *Chem. Commun.*, 2007, 3814–3816.
73 E. R. Johnson, S. Keinan, P. Mori-Sanchez, J. Contreras-Garcia, A. J. Cohen and W. Yang, *J. Am. Chem. Soc.*, 2010, **132**, 6498–6506.
74 J. Contreras-Garcia, E. R. Johnson, S. Keinan, R. Chaudret, J.-P. Piquemal, D. N. Beratan and W. Yang, *J. Chem. Theory Comput.*, 2011, **7**, 625–632.
75 G. Saleh, L. L. Presti, C. Gatti and D. Ceresoli, *J. Appl. Crystallogr.*, 2013, **46**, 1513–1517.
76 G. Saleh, C. Gatti, L. L. Presti and J. Contreras-Garc, *Chem. – Eur. J.*, 2012, **18**, 15523–15536.
77 M. P. Johansson and M. Swart, *Phys. Chem. Chem. Phys.*, 2013, **15**, 11543–11553.
78 C. B. Hubschle and B. Dittrich, *J. Appl. Crystallogr.*, 2011, **44**, 238–240.
79 F. H. Allen, *Acta Crystallogr., Sect. B: Struct. Sci.*, 2002, **58**, 380–388.